SUPPLEMENTAL MATERIALS AND METHODS

Western blot, Quantitative reverse-transcription polymerase chain reaction (qRT-PCR), Chromatin immunoprecipitation

Western blots were performed as described (Frank et al., 2011). Primary antibodies used in this study include p53 (CM5, Leica Microsystems, NCL-p53-CM5p), Gapdh(14C10, Cell Signaling, 2118), Actin (AC-15, Sigma, A5441), Akt (Cell Signaling, 9272), phospho-Akt (Ser473, Cell Signaling, 9271), Pck1 (Abcam, ab28455), Ccl2 (Abcam, ab25124). qRT-PCR analyses were performed as described (Kung et al., 2014). Primer pairs used for qRT-PCR analysis are listed in Supplemental Information. Chromatin from the mouse liver was isolated as described previously with minor modifications (Rubins et al., 2005). In brief, approximately 200 mg of mouse livers were minced in cold PBS and cross-linked in 1% freshly-made paraformaldehyde-PBS for 10 min with constant shaking. Cross-linking was quenched by the addition of glycine to a final concentration of 125 mM, with constant shaking, for 5 min. The tissue was rinsed in cold PBS and homogenized with a Dounce homogenizer into single cell suspension in 3.5 ml cold cell lysis buffer (10 mM Tris-Cl, pH 8.0, 10 mM NaCl, 3 mM $MgCl_2$, 1% NP-40) supplemented with protease inhibitors (Roche, #04693159001). Cells were incubated on ice for 10 min before being spun down by centrifugation at 1,000 × g for 5 min at 4°C to pellet nuclei. The pellet was then resuspended in nuclear lysis buffer (1% SDS, 5 mM EDTA, 50 mM Tris-Cl, pH 8.0) supplemented with protease inhibitors. Chromatin was sheared by sonication to an average size of ~200 to 1000 bp using a Sonic Dismembrator (model 150, Fisher Scientific) at 30% magnitude, 30-sec-on/1-min-off cycle for 12 cycles. Insoluble debris was removed by centrifugation at 13,000 × g for 15 min at 4°C, and supernatant containing chromatin was stored in -80°C. Chromatin immunoprecipitation analysis was performed according to the manufacturer's protocol (EZ-ChIP; Millipore). p53 responsive elements (REs) in the mouse *Pck1*, *Ccl2*, *Tnf* and *Npc1l1* genes were either reported previously (*Tnf*) or predicted (*Pck1*, *Ccl2*, *Npc1l1*) through MatInspector software of Genomatix using the consensus p53 binding

sequence RRRCWWGYYY (R=A or G; W =A or T; Y = C or T), allowing no more than 2 mismatches (Cartharius et al., 2005; Lujambio et al., 2013). Primer pairs used for ChIP analysis are listed at the end of Supplemental Information.

Immunofluorescence staining of pancreata

Cryosections of pancreas were permeabilized with 0.25% Triton X-100 in DPBS buffer for 10 mins, blocked in blocking buffer for 1 h (5% goat serum, 0.5 g BSA in 50 ml DPBS) and then incubated in the primary antibody (or sequential incubation for co-staining) for 1 h at 37°C, followed by application of a fluorescence-conjugated secondary antibody for 1 h at 37°C (Jackson ImmunoResearch Laboratories, Rhodamine Red-X-AffiniPure Goat Anti-Rabbit IgG, 111-295-144; Alexa Fluor 488-AffiniPure Goat Anti-Mouse IgG, 115-545-003). Nuclei were counterstained with DAPI. Stained samples were imaged using a Leica TCS SP5 II scanning laser confocal system (Wistar Institute Imaging Facility). Quantification of images was performed using ImageJ or NIS elements software (Nikon). Primary antibodies used include insulin (Abcam, ab8304 and ab181547), glucagon (Abcam, ab10988), somatostatin (Thermo Scientific, MA5-16987), and Ki67 (Abcam, ab15580).

Energy expenditure monitoring using metabolic cages

Indirect calorimetry was performed to assess energy expenditure and basic metabolic capabilities (Oxyman/Comprehensive Laboratory Animal Monitoring System – CLAMS; Columbus Instruments). Five-week old mice were single caged with water and food *ad libitum*. After 2 days of acclimation period, oxygen consumption (VO_2) and carbon dioxide production (VCO_2) were measured for 48 h using an air flow of 600 ml/min and an ambient temperature of 22°C. The respiratory exchange ratio (RER) was calculated as VCO_2/VO_2. Heat (kcal/h) = 3.815 + 1.232 × RER. Ambulatory and total activities were measured simultaneously with photodetectors (Optovarimex System; Columbus Instruments).

Senescence-associated β-Galactosidase, Sirius Red and Oil Red staining

Pancreas tissue was embedded in NEG 50^{TM} (Thermo Scientific, 6502) and flash-frozen in liquid nitrogen immediately after it was harvested. The tissues were then sectioned and stained with β-galactosidase as described (Webster et al., 2015). For Sirius red staining, pancreas and liver tissue sections were deparaffinized, rehydrated and stained by Picrosirius Red solution (American Master Tech Scientific, Lodi, CA). Slides were incubated overnight at room temperature, and washed twice with acidic water (5 ml of glacial acetic acid diluted in 1 liter of distilled water) the next day. Slides were then dehydrated in butanol and xylene, mounted using a xylene-based mounting solution, and visualized with light microscopy (E600 upright microscope, Nikon). For oil red staining, a stock solution was made with 0.5 g of Oil Red O (Sigma, O0625) dissolved in 100 ml of isopropanol. Thirteen-millimeter-thick frozen liver sections were air-dried and fixed in 10% formalin (Pharmco, 8BUFF-FORM) for 10 min at RT. After brief wash with water for 1 min, samples were rinsed with 60% isopropanol for 5 min. Staining was performed with freshly prepared Oil Red O working solution (Mix stock stain solution with water at 3:2 ratios before filtering it through 0.45 μm filters) for 15 min. Stained samples were washed with 60% isopropanol for 5 min, followed by brief counterstain of haematoxylin. Distilled water was used for the final wash and samples were mounted in aqueous mounting medium (Vector Laboratories, H-1000). Quantification of stained images was performed using NIS elements software (Nikon).

Immunohistochemical (IHC) analysis

Immunohistochemical (IHC) analysis was conducted by using EnVision System and the Peroxidase kit (Dako, Carpinteria, CA) following the manufacturer's instructions. Briefly, paraffin-embedded tissue sections were de-paraffinized in xylene (Fisher, X5-SK4) and re-hydrated in ethanol (100%-95%-85%-75%) and then distilled water. Samples were then subjected to antigen retrieval by steaming in target retrieval solution, pH 9.0 (Dako, S2367) for 45 minutes. After quenching endogenous peroxidase activity with 3% hydrogen peroxide (Fisher, BP2633), nonspecific protein binding was

blocked with 1% bovine serum albumin. Tissue sections were incubated overnight with primary antibody at 4°C, followed by HRP-conjugated anti-mouse/anti-rabbit IgG for 1 hour at RT. Antibody complexes were then detected and visualized by adding the substrate and chromogen 3,3′-diaminobenzidine. Primary antibodies used in IHC staining include Pck1 (Abcam, ab28455), Ccl2 (Abcam, ab25124), F4/80 (Abcam, ab6640), NF-κB p65 (phosphor-S276) (Abcam, ab194726), and Tnf (Abcam, ab6671). Sections were then lightly counterstained with haematoxylin (Dako, S3309) before visualized using widefield E600 upright microscope (Nikon) with ImagePro Plus software. Cells showing positive signals were counted in at least 6 high-power fields. Quantification of images was performed using either NIS elements software (Nikon) or blinded counting.

Mouse primers used in quantitative real-time PCR assays

Gene	Forward primer 5'-3'	Reverse primer 5'-3'
Ppia(Cyclophilin A)	GGGTTCCTCCTTTCACAGAA	GATGCCAGGACCTGTATGCT
Cdkn1a(p21)	TTGCACTCTGGTGTCTGAGC	GTGGGCACTTCAGGGTTTT
Mdm2	CGAGCTCTCAGATGAGGATG	GATGGAAGGGGAGGATTCAT
Pmaip1(Noxa)	TCAACTCAGGAAGATCGGAGA	TGAGCACACTCGTCCTTCAA
Dram1	CCTGCAATCGATCATCTCCT	TTTGGATTCCATTCCAGCTT
Pgm2	CGACACCGACAGAGACACC	ACCTCCAGCAATGAGCTGTT
Igfbp3	CAGGCAGCCTAAGCACCTAC	GCATGGAGTGGATGGAACTT
Prkab2	GGGAAAGGAGCACAAGATCA	CTGCTGCCAGGGTACAAACT
Sesn1	ATTCTGAAGAGCGTCGAGGA	ATGCATCTGTGCGTCTTCAC
Sesn2	CATTCCGAGATCAAGGGCTA	CCGAAGGATCTCTTCCACTG
Pten	ACACCGCCAAATTTAACTGC	TACACCAGTCCGTCCCTTTC
G6pc	AGCAGTTCCCTGTCACCTGT	TGGCTTTTTCTTTCCTCGAA
Pck2	CCATGGCTGCTATGTACCTC	GCCACAAAGTCTCGAACTCC
Aqp3	CATGGGTCGACAGAAGGAGT	CCAAAAGCCAAGTTGATGGT
Aqp9	TCAGTCGAGAAAAGGCTGGT	GAACCACTCCATCCTTCCAA
Ppargc1a	AAAAGCTTGACTGGCGTCAT	TCAGGAAGATCTGGGCAAAG
Ppargc1b	CCGAGCTCTTCCAGATTGAC	TTCATCCAGTTCTGGGAAGG
Gamt	TTGGGAGACCCCCTATATGC	AAGACCCCATCATTGCACTC
Pck1	TGGATGTCGGAAGAGGACTT	CACATAGGGCGAGTCTGTCA
Apom	AACTAACTGCGCTGGGAATG	ATTGTCCACCGGATCAAAAG
Lpin1	TTGCACATGAAGTTGGGAGA	CTTCAGCTGGCTTTCCATTC
Npc1l1	TGGACTGGAAGGACCATTTC	AAGGAAGGGGAAGACAGGTG
Ccl2	CCCAATGAGTAGGCTGGAGA	TCTGGACCCATTCCTTCTTG
Ccl4	CCCACTTCCTGCTGTTTCTC	GTCTGCCTCTTTTGGTCAGG
Adgre1(F4/80)	GGATGTACAGATGGGGGATG	GGAAGCCTCGTTTACAGGTG
Tnf	CCCCAAAGGGATGAGAAGTT	CACTTGGTGGTTTGCTACGA
Cd68	CCAATTCAGGGTGGAAGAAA	CTCGGGCTCTGATGTAGGTC
Cxcl10	AAGTGCTGCCGTCATTTTCT	CCTATGGCCCTCATTCTCAC
Adipoq	GGAACTTGTGCAGGTTGGAT	CCAAGAAGACCTGCATCTCC
Pde3b	GACCGTCGTTGCCTTGTATT	CTCCATTTCCACCTCCAGAA
Timp1	GCATCTGGCATCCTCTTGTT	TGGGGAACCCATGAATTTAG
Acta2	CTGACAGAGGCACCACTGAA	AGAGGCATAGAGGGACAGCA
Col1a1	TGTTCAGCTTTGTGGACCTC	TCAAGCATACCTCGGGTTTC

Mouse primers used in ChIP analyses

Target gene	Forward primer 5'-3'	Reverse primer 5'-3'
Pck1-RE1	GTCTCGTGGCTTCTGAGGAC	CCATGTCCACAGCTCATGTC
Pck1-RE2	GGCAGGGTCATTTCATTCAC	CGGTCCTTCCGTAGACTTTG
Pck1-RE3	ATGCCCTGTGAGGTTAGCAT	GGGAAACAAGGACAACAGGA
Ccl2-RE1	CAGGAAATGCTTGGATGACA	GGTGGAAAGGACCAGACTCA
Ccl2-RE2	CATAGCCAAGCCACTGTGAA	GACCTCCATGCTGAAGTGCT
Npc1l1-RE1	AGAGATTGAGGGCAATGGAG	GGGTCACCTGGTCTCACATC
Npc1l1-RE2	GTGGGACTTGCCACTCAGA	CCTTCACCCTTCCTCCTGA
Tnf	GCCTCTCCTACCCTGTCTCC	CAGGAGGACCAGACCCATTA

SUPPLEMENTAL REFERENCES

Cartharius, K., Frech, K., Grote, K., Klocke, B., Haltmeier, M., Klingenhoff, A., Frisch, M., Bayerlein, M., and Werner, T. (2005). MatInspector and beyond: promoter analysis based on transcription factor binding sites. Bioinformatics *21*, 2933-2942.

Frank, A.K., Leu, J.I., Zhou, Y., Devarajan, K., Nedelko, T., Klein-Szanto, A., Hollstein, M., and Murphy, M.E. (2011). The codon 72 polymorphism of p53 regulates interaction with NF-{kappa}B and transactivation of genes involved in immunity and inflammation. Molecular and cellular biology *31*, 1201-1213.

Kung, C.P., Khaku, S., Jennis, M., Zhou, Y., and Murphy, M.E. (2014). Identification of TRIML2, a Novel p53 Target, that Enhances p53-SUMOylation and Regulates the Transactivation of Pro-apoptotic Genes. Mol Cancer Res.

Lujambio, A., Akkari, L., Simon, J., Grace, D., Tschaharganeh, D.F., Bolden, J.E., Zhao, Z., Thapar, V., Joyce, J.A., Krizhanovsky, V.*, et al.* (2013). Non-cell-autonomous tumor suppression by p53. Cell *153*, 449-460.

Rubins, N.E., Friedman, J.R., Le, P.P., Zhang, L., Brestelli, J., and Kaestner, K.H. (2005). Transcriptional networks in the liver: hepatocyte nuclear factor 6 function is largely independent of Foxa2. Mol Cell Biol *25*, 7069-7077.

Webster, M.R., Xu, M., Kinzler, K.A., Kaur, A., Appleton, J., O'Connell, M.P., Marchbank, K., Valiga, A., Dang, V.M., Perego, M.*, et al.* (2015). Wnt5A promotes an adaptive, senescent-like stress response, while continuing to drive invasion in melanoma cells. Pigment Cell Melanoma Res *28*, 184-195.

Supplemental Figure Legends

Figure S1. Young P72 and R72 mice share similar energy metabolism profiles. Related to Figure 1.

A–D) Indirect calorimetry was used to measure metabolic profiles of 4-week old P72 (blue line) and R72 (red line) mice during a 48-hour period. Assays include: oxygen consumption (VO_2) (A), carbon dioxide release (VCO_2) (B), respiratory exchange ratio (RER, VCO_2/CO_2) (C), and energy expenditure (D), n=4 each genotype.

E) Food intake of CD-fed 4-week old P72 and R72 mice was measured during a 48-hour period, n=4 each genotype.

F) Ambulatory activity of CD-fed 4-week old P72 and R72 mice over a 48-hour period, n=4 each genotype.

G) Total activity of CD-fed 4-week old P72 and R72 mice over a 48-hour period, n=4 each genotype.

Figure S2. R72 mice develop more severe insulin resistance after HFD. Related to Figure 2.

A) GTT results in P72 mice after CD and HFD, n=20. Error bars mark standard error.

B) GTT results in R72 mice after CD and HFD, n=20. Error bars mark standard error.

C) Quantification of area under the curve (AUC) after CD and HFD, n=20. Error bars mark standard error.

D) Quantification of area under the curve (AUC) increase after HFD, n=20. Error bars mark standard error.

E) Average numbers of islets per mm^2 in pancreas of HFD-fed P72 and R72 mice, n=5 each genotype. Error bars mark standard error.

F) Immunofluorescence staining of endocrine cells in the pancreata of HFD-fed mice. Detection of insulin, glucagon and somatostatin was performed to identify β-, α- and δ-cells, respectively. Dashed lines mark pancreatic islets of Langerhans. Scale bar, 50 μm.

G) Percentage of each endocrine cell population in the pancreatic islets of HFD-fed mice, n=5. Error bars mark standard error.

H) Percentage of Ki67-positive cells in pancreatic islets of HFD-fed mice, n=5. Error bars mark standard error.

I) Senescence-associated β-galactosidase staining in pancreas of P72 and R72 mice after HFD. Note increased islet size and SA β-gal staining in R72. Scale bar, 200 μm.

J) Glucose disappearance rate during hyperinsulinemic-euglycemic clamp analysis after HFD, n=8.

K) Hepatic glucose production (HGP) suppression during hyperinsulinemic-euglycemic clamp analysis after HFD, n=8.

L) 2-deoxyglucose uptake rate in adipose tissue during hyperinsulinemic-euglycemic clamp analysis after HFD, n=8.

M) 2-deoxyglucose uptake in gastrocnemius muscle during hyperinsulinemic-euglycemic clamp analysis after HFD, n=8.

N) 2-deoxyglucose uptake rate in brown adipose tissue during hyperinsulinemic-euglycemic clamp analysis after HFD, n=8.

Figure S3. Increased inflammation in the adipose tissue and livers of R72 mice after HFD. Related to Figure 3.

A) Immunohistochemical staining of F4/80 (macrophage marker) in adipose tissue of Hupki mice after HFD. Scale bar, 50 μm.

B) Quantification of F4/80-positive cells in A), n=5. Error bars mark standard error. The double asterisk denotes $p<0.005$.

C) Immunohistochemical staining of phosphorylated NFκB/p65 (S276) as an inflammation marker (marked by arrowheads) in the livers of Hupki mice after HFD. Scale bar, 50 μm.

D) Quantification of phospho-NFκB/p65-positive cells in C) and normalized to the number of hepatocytes, n=5. Error bars mark standard error. The asterisk denotes $p <0.05$.

E) Immunohistochemical staining of F4/80 in the livers of Hupki mice after HFD. Scale bar, 50 μm.

F) Quantification of F4/80-positive cells in E) and normalized to the number of hepatocytes, n=5. Error bars mark standard error.

Figure S4. The codon 72 polymorphism of p53 differentially regulates expression of p53-regulated genes involved with lipid metabolism and inflammation. Related to Figure 4.

A) Western blot analysis for Pck1 protein in three HFD-fed mice of each genotype. Gapdh was used as the loading control.

B) Quantification of Pck1 expression in A) using ImageJ software and normalized to Gapdh. Error bars mark standard error. The double asterisk denotes $p<0.005$.

C) Immunohistochemical staining of Pck1 in the livers of Hupki mice after HFD. Arrowheads mark positive cells. Scale bar, 50 μm.

D) Quantification of Pck1 staining in the livers of Hupki mice after HFD, n=5 each genotype. The triple asterisk denotes $p<0.0005$.

E) Western blot analysis for Ccl2 protein level in three HFD-fed mice of each genotype. Actin was used as the loading control.

F) Quantification of Ccl2 expression in E) using ImageJ software and normalized to Actin. Error bars mark standard error. The asterisk denotes $p <0.05$.

G) Immunohistochemical staining of Ccl2 in the livers of Hupki mice after HFD. Arrowheads mark positive cells. Scale bar, 50 μm.

H) Quantification of Ccl2 staining in the livers of Hupki mice after HFD, n=5 each genotype. The asterisk denotes $p<0.05$.

I) Immunohistochemical staining of Tnf in the livers of Hupki mice after HFD. Arrow heads mark positive cells. Scale bar, 50 μm.

J) Quantification of Tnf staining in the livers of Hupki mice after HFD, n=5 each genotype. The asterisk denotes $p<0.05$.

Figure S5. Similar inflammation status in adipose tissue and liver between P72 and R72 mice after Long Chow Diet (LCD). Related to Figure 5.

A) H&E staining of adipose tissues after LCD. Scale bar, 50 μm.

B) IHC staining of F4/80 (macrophage marker) in adipose tissue (marked by arrowheads) of Hupki mice after LCD. Scale bar, 50 μm.

C) Quantification of F4/80-positive cells in B), n=5 each genotype. Error bars mark standard error.

D) IHC staining of phosphorylated NFκB/p65 (S276) as an inflammation marker (marked by arrowheads) in the livers of Hupki mice after LCD. Scale bar, 50 μm.

E) Quantification of phospho-NFκB/p65-positive cells in D) and normalized to the number of hepatocytes, n=5 each genotype. Error bars mark standard error.

F) IHC staining of F4/80 (macrophage marker) in the livers of Hupki mice after LCD. Scale bar, 50 μm.

G) Quantification of F4/80-positive cells in F) and normalized to the number of hepatocytes, n=5 each genotype. Error bars mark standard error.

Figure S6. A short-term HFD in P72 and R72 mice reveals a subset of 'early responder' p53-regulated genes. Related to Figure 6.

A) Western analysis of whole cell lysate from the livers of Hupki mice before (control) or after SHFD for p53 and Gapdh.

B) Quantifications of signal intensities in A) using ImageJ software. The level of p53 was normalized to Gapdh. Protein levels in control P72 samples were set as 1-fold.

C) qRT-PCR of the p53 target genes *Cdkn1a(p21)* and *Pmaip1*(*Noxa*) in 4-week-old Hupki mice before SHFD, n=4. Error bars mark standard error.

D) qRT-PCR of the p53-regulated genes associated with lipid metabolism in 4-week-old Hupki mice before SHFD, n=4. Error bars mark standard error.

E) qRT-PCR of the p53-regulated genes associated with inflammation in 4-week-old Hupki mice before SHFD, n=4. Error bars mark standard error.

F) IHC staining of Tnf in Hupki mouse adipose tissue before and after SHFD (marked by arrow heads). Note after SHFD, the increase in Tnf staining is marked. Scale bar, 50 μm.

G) H&E staining of livers before and after SHFD. Red arrow heads mark visible liver vacuolization. Scale bar, 100 μm.

H) IHC staining of phosphorylated NFκB/p65 (S276) as an inflammation marker (marked by arrowheads) in the livers of Hupki mice before and after SHFD. Scale bar, 50 μm.

I) IHC staining of F4/80 (macrophage marker) in the livers of Hupki mice before and after SHFD. Scale bar, 50 μm.

Figure S7. Tnf and Npc1l1 inhibition rescues R72-increased weight gain after Short-term HFD (SHFD). Related to Figure 7.

Quantification of percentage of weight gain after SHFD with or without treatments of C87 or Ezetimibe, n=5 each genotype and treatment. Error bars mark standard error. The asterisk denotes $p<0.05$.

Figure S1

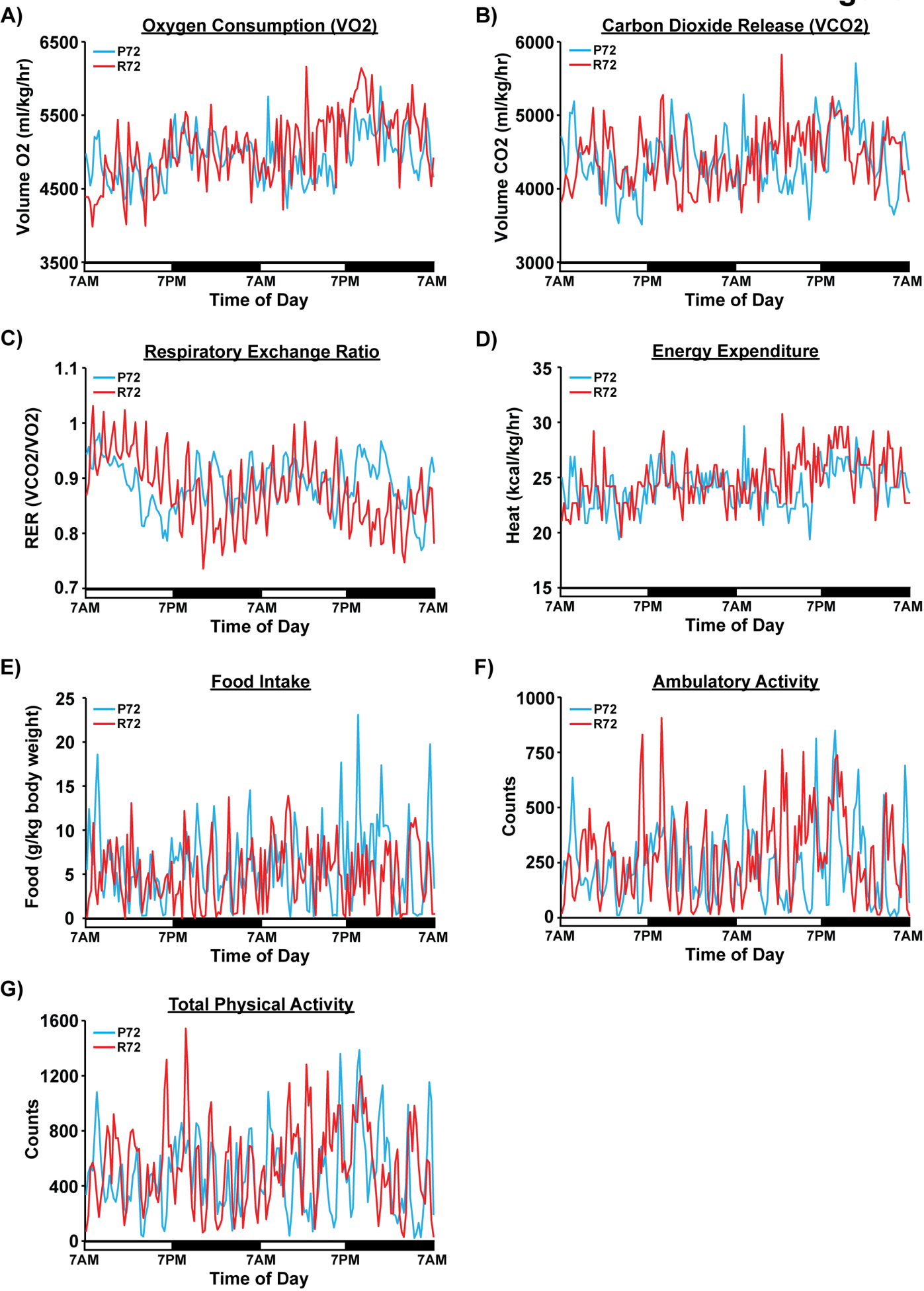
A)
Oxygen Consumption (VO2)
Volume O2 (ml/kg/hr)
6500
5500
4500
3500
P72
R72
7AM
7PM
7AM
7PM
7AM
Time of Day
B)
Carbon Dioxide Release (VCO2)
Volume CO2 (ml/kg/hr)
6000
5000
4000
3000
P72
R72
7AM
7PM
7AM
7PM
7AM
Time of Day
C)
Respiratory Exchange Ratio
RER (VCO2/VO2)
1.1
1
0.9
0.8
0.7
P72
R72
7AM
7PM
7AM
7PM
7AM
Time of Day
D)
Energy Expenditure
Heat (kcal/kg/hr)
35
30
25
20
15
P72
R72
7AM
7PM
7AM
7PM
7AM
Time of Day
E)
Food Intake
Food (g/kg body weight)
25
20
15
10
5
0
P72
R72
7AM
7PM
7AM
7PM
7AM
Time of Day
F)
Ambulatory Activity
Counts
1000
750
500
250
0
P72
R72
7AM
7PM
7AM
7PM
7AM
Time of Day
G)
Total Physical Activity
Counts
1600
1200
800
400
0
P72
R72
7AM
7PM
7AM
7PM
7AM
Time of Day

Figure S2

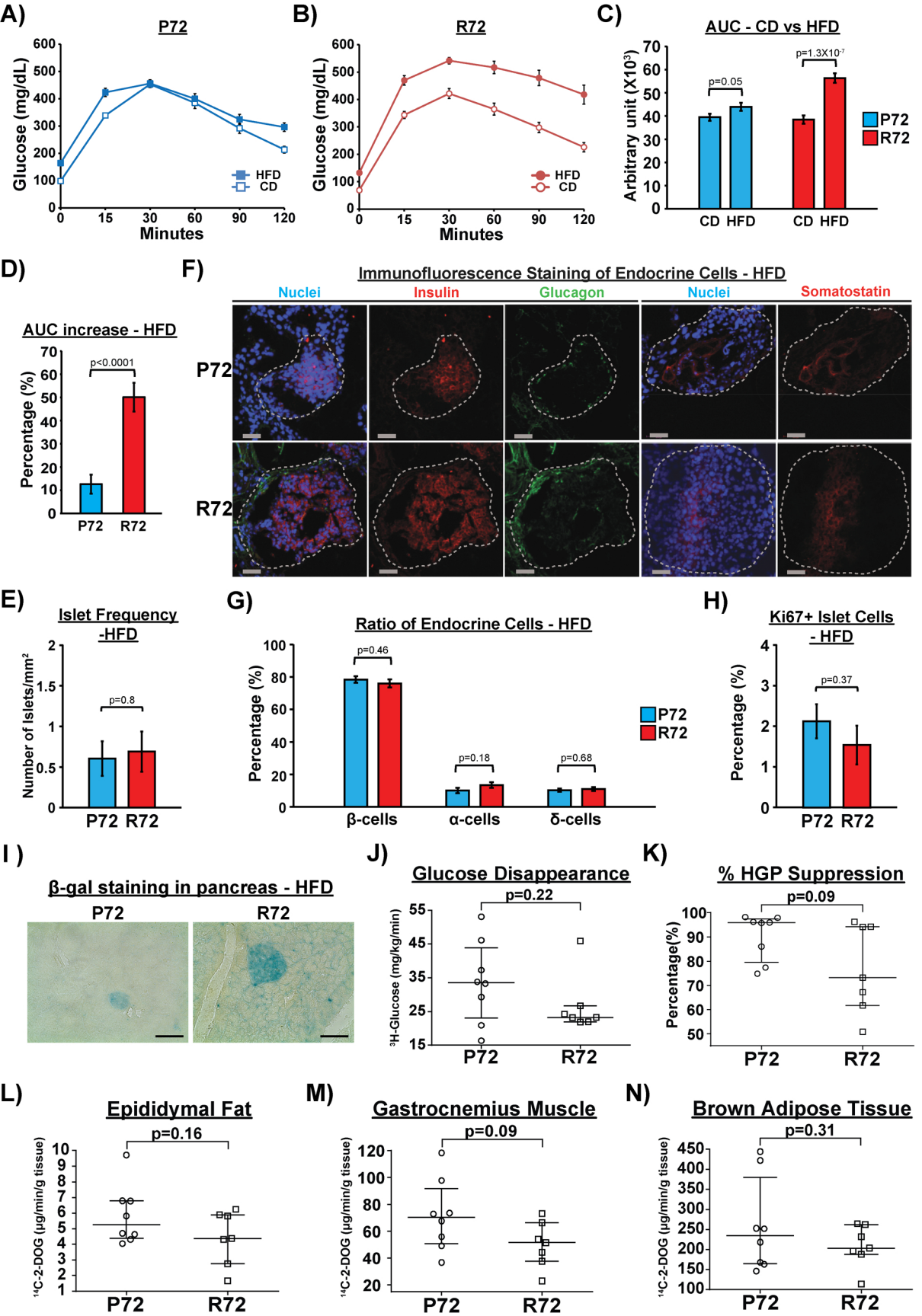
A)
P72
Glucose (mg/dL)
Minutes
HFD
CD
B)
R72
C)
AUC - CD vs HFD
Arbitrary unit (X10³)
p=0.05
p=1.3X10⁻⁷
P72
R72
CD HFD CD HFD
D)
AUC increase - HFD
Percentage (%)
p<0.0001
P72 R72
F)
Immunofluorescence Staining of Endocrine Cells - HFD
Nuclei
Insulin
Glucagon
Nuclei
Somatostatin
P72
R72
E)
Islet Frequency -HFD
Number of Islets/mm²
p=0.8
P72 R72
G)
Ratio of Endocrine Cells - HFD
Percentage (%)
p=0.46
p=0.18
p=0.68
β-cells
α-cells
δ-cells
P72
R72
H)
Ki67+ Islet Cells - HFD
Percentage (%)
p=0.37
P72 R72
I)
β-gal staining in pancreas - HFD
P72
R72
J)
Glucose Disappearance
³H-Glucose (mg/kg/min)
p=0.22
P72
R72
K)
% HGP Suppression
Percentage(%)
p=0.09
P72
R72
L)
Epididymal Fat
¹⁴C-2-DOG (µg/min/g tissue)
p=0.16
P72
R72
M)
Gastrocnemius Muscle
¹⁴C-2-DOG (µg/min/g tissue)
p=0.09
P72
R72
N)
Brown Adipose Tissue
¹⁴C-2-DOG (µg/min/g tissue)
p=0.31
P72
R72

Figure S3

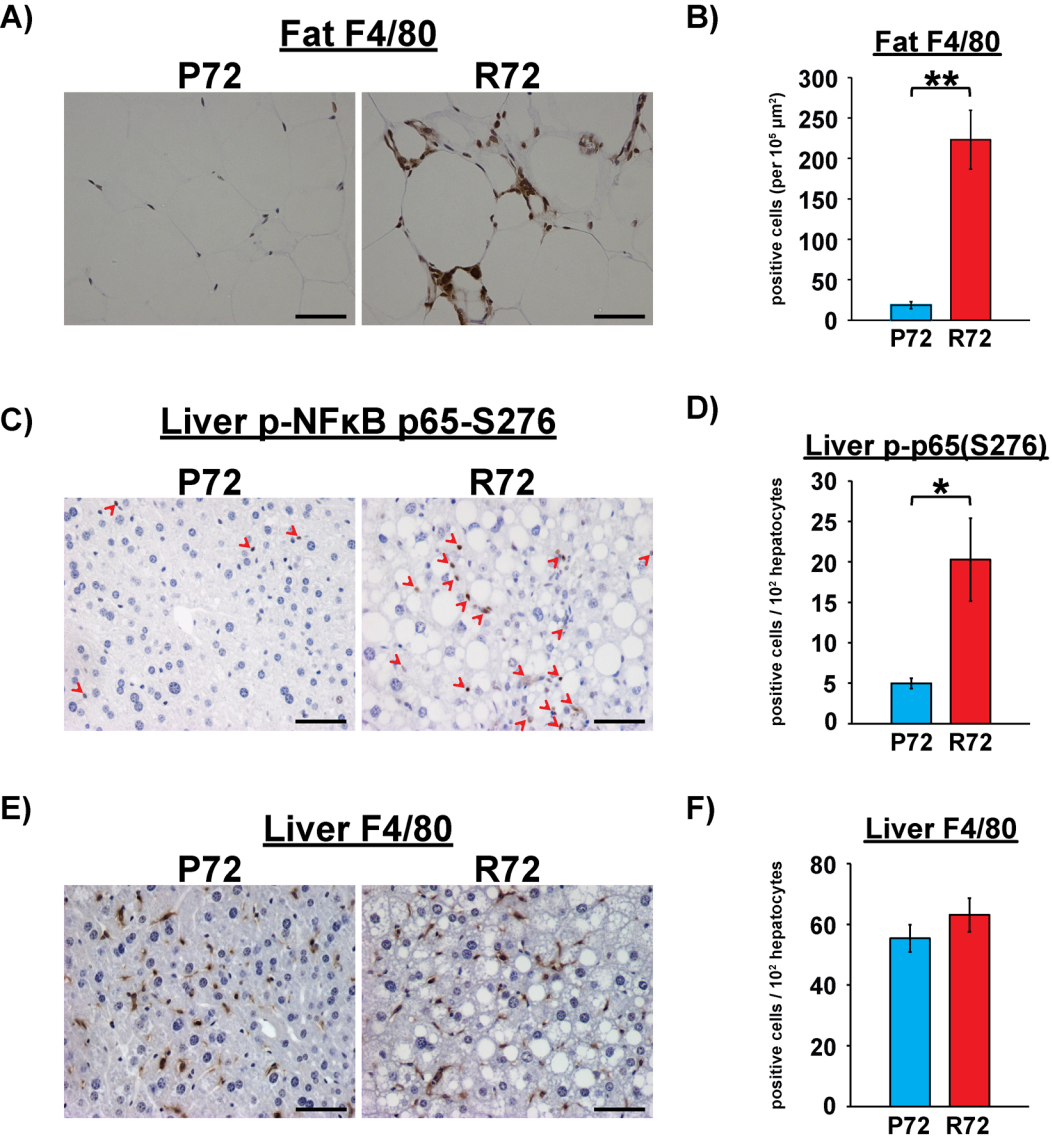
A)
Fat F4/80
P72
R72
B)
Fat F4/80
**
positive cells (per 10⁵ µm²)
300
250
200
150
100
50
0
P72
R72
C)
Liver p-NFκB p65-S276
P72
R72
D)
Liver p-p65(S276)
*
positive cells / 10² hepatocytes
30
25
20
15
10
5
0
P72
R72
E)
Liver F4/80
P72
R72
F)
Liver F4/80
positive cells / 10² hepatocytes
80
60
40
20
0
P72
R72

Figure S4

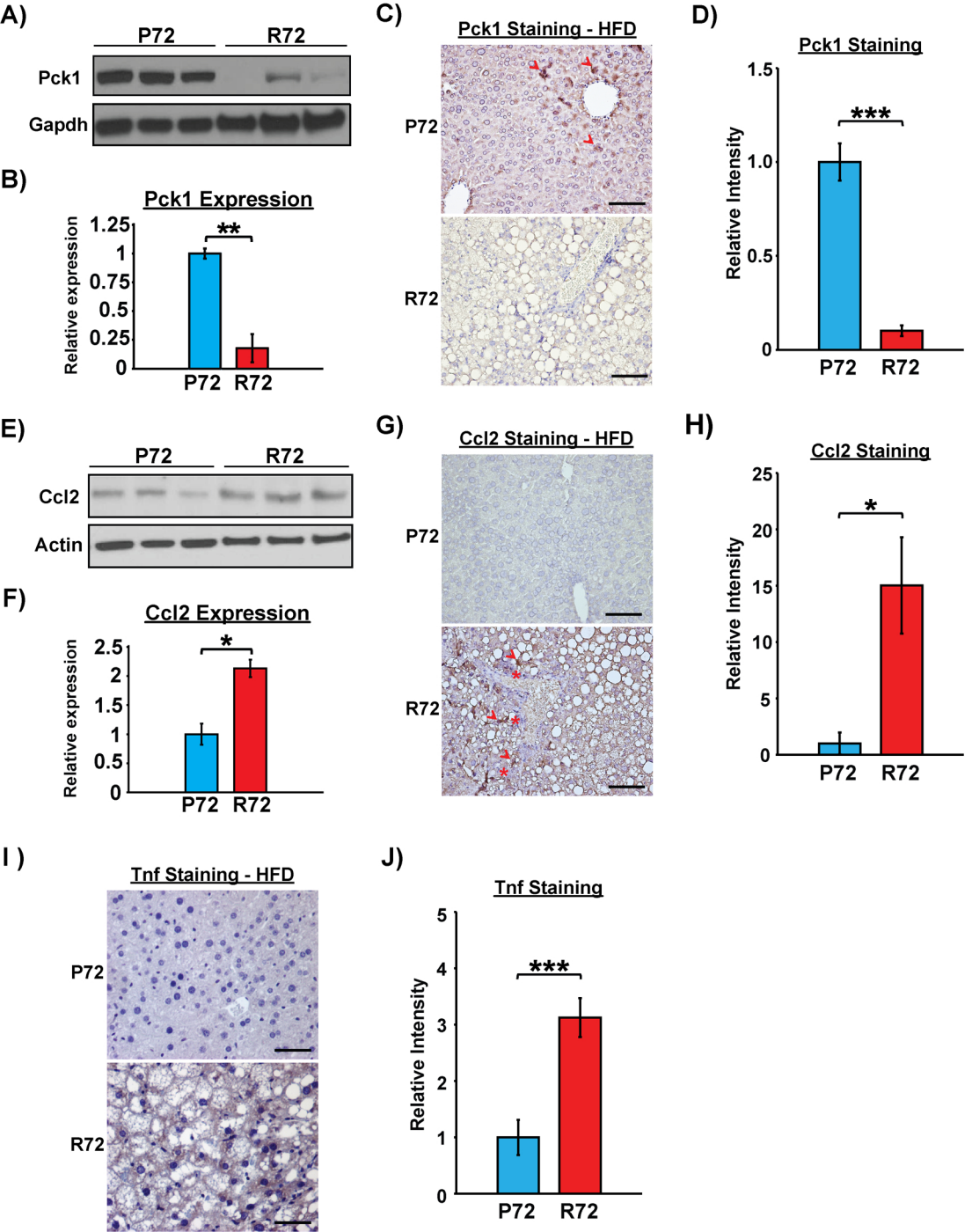
A)
P72
R72
Pck1
Gapdh
B)
Pck1 Expression
Relative expression
1.25
1
0.75
0.5
0.25
0
**
P72
R72
C)
Pck1 Staining - HFD
P72
R72
D)
Pck1 Staining
Relative Intensity
1.5
1.0
0.5
0
***
P72
R72
E)
P72
R72
Ccl2
Actin
F)
Ccl2 Expression
Relative expression
2.5
2
1.5
1
0.5
0
*
P72
R72
G)
Ccl2 Staining - HFD
P72
R72
H)
Ccl2 Staining
Relative Intensity
25
20
15
10
5
0
*
P72
R72
I)
Tnf Staining - HFD
P72
R72
J)
Tnf Staining
Relative Intensity
5
4
3
2
1
0
***
P72
R72

Figure S5

A)

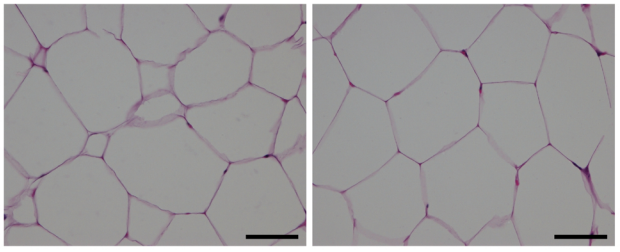

B)

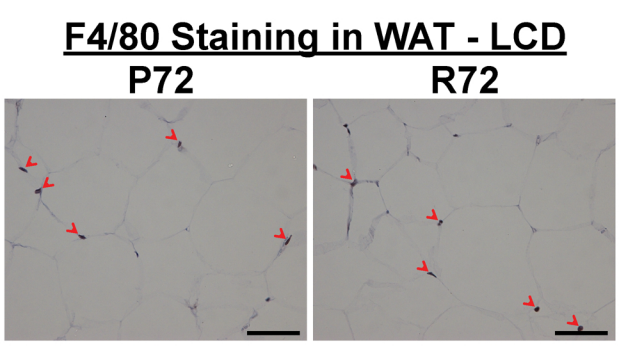

C)

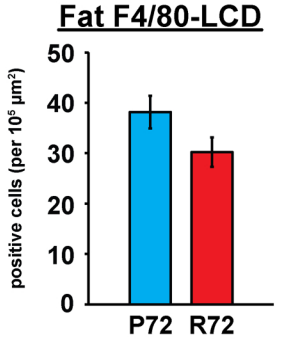

D)

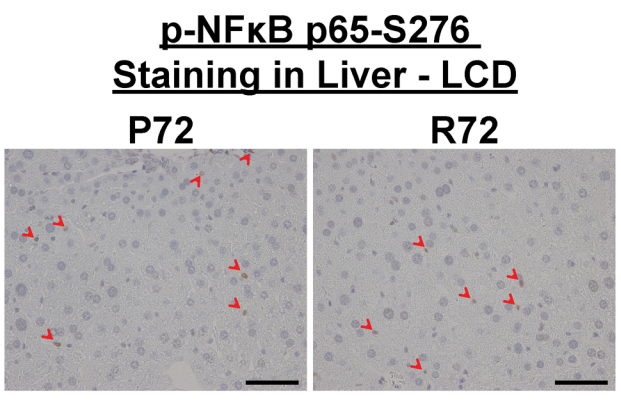

E)

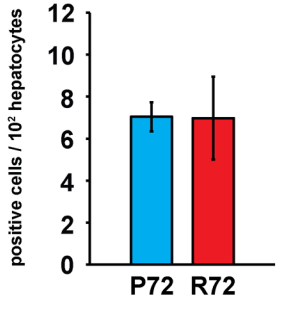

F)

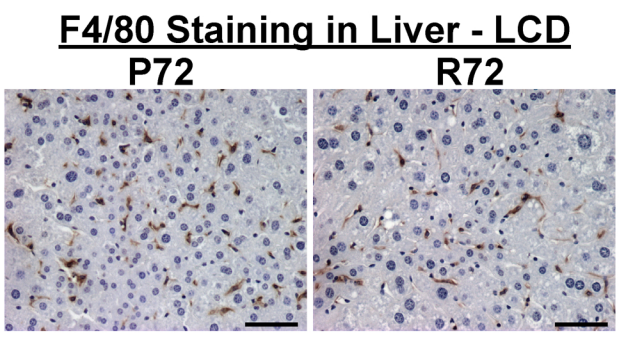

G)

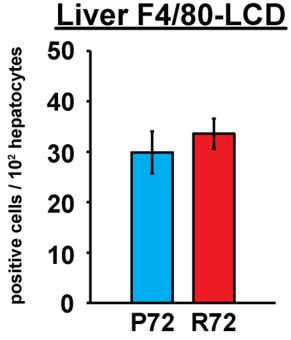

Figure S6

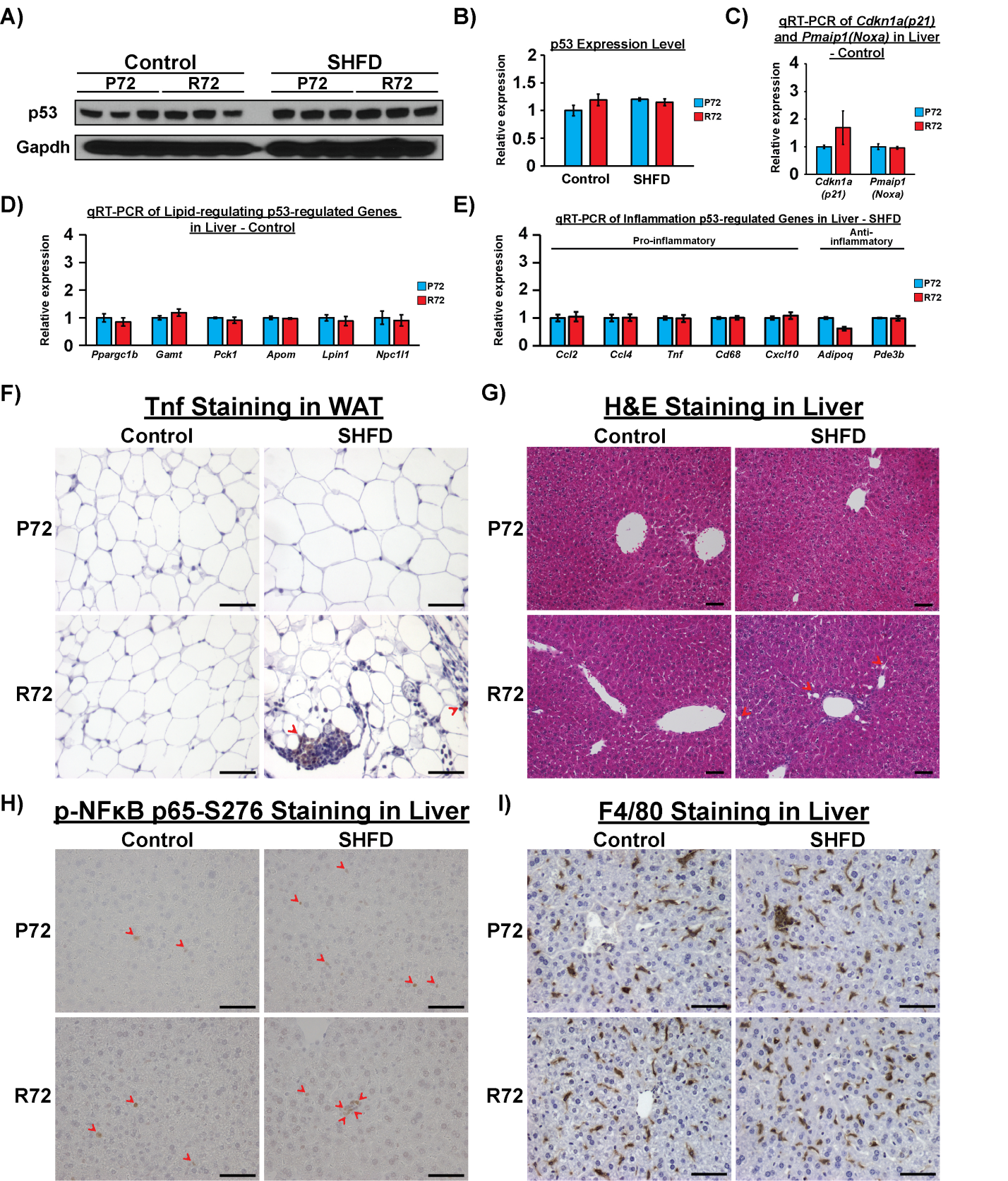
A)
Control
SHFD
P72
R72
P72
R72
p53
Gapdh
B)
p53 Expression Level
Relative expression
2
1.5
1
0.5
0
Control
SHFD
P72
R72
C)
qRT-PCR of Cdkn1a(p21) and Pmaip1(Noxa) in Liver - Control
Relative expression
4
3
2
1
0
Cdkn1a (p21)
Pmaip1 (Noxa)
P72
R72
D)
qRT-PCR of Lipid-regulating p53-regulated Genes in Liver - Control
Relative expression
4
3
2
1
0
Ppargc1b
Gamt
Pck1
Apom
Lpin1
Npc1l1
P72
R72
E)
qRT-PCR of Inflammation p53-regulated Genes in Liver - SHFD
Pro-inflammatory
Anti-inflammatory
Relative expression
4
3
2
1
0
Ccl2
Ccl4
Tnf
Cd68
Cxcl10
Adipoq
Pde3b
P72
R72
F)
Tnf Staining in WAT
Control
SHFD
P72
R72
G)
H&E Staining in Liver
Control
SHFD
P72
R72
H)
p-NFκB p65-S276 Staining in Liver
Control
SHFD
P72
R72
I)
F4/80 Staining in Liver
Control
SHFD
P72
R72

Figure S7

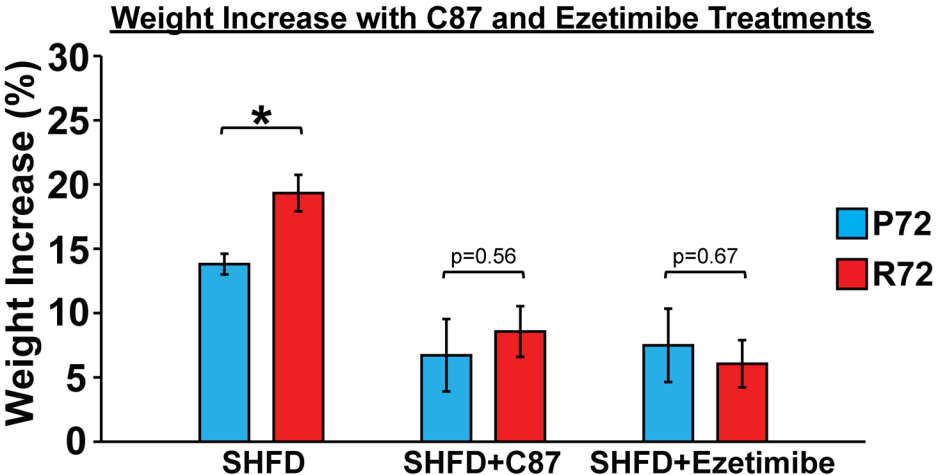
Weight Increase with C87 and Ezetimibe Treatments
Weight Increase (%)
30
25
20
15
10
5
0
*
p=0.56
p=0.67
P72
R72
SHFD
SHFD+C87
SHFD+Ezetimibe